Enhancing Intracellular Accumulation and Target Engagement of PROTACs with Reversible Covalent Chemistry

Wen-Hao Guo,[1,†] Xiaoli Qi,[1,†] Xin Yu,[1] Yang Liu,[2] Chan-I Chung,[3] Fang Bai,[4] Xingcheng Lin,[5] Dong Lu,[1] Lingfei Wang,[1] Jianwei Chen,[1] Lynn Hsiao Su,[1] Krystle J. Nomie,[2] Feng Li,[6,7] Meng C. Wang,[8,9,10] Xiaokun Shu,[3] José N. Onuchic,[4] Jennifer A. Woyach,[11] Michael L. Wang,[2] and Jin Wang[1,7,12]*

1. Department of Pharmacology and Chemical Biology, Baylor College of Medicine, Houston TX 77030, USA.

2. Department of Lymphoma/Myeloma, Division of Cancer Medicine, The University of Texas MD Anderson Cancer Center, Houston, TX 77030, USA.

3. Department of Pharmaceutical Chemistry, University of California−San Francisco, San Francisco, CA 94158, USA.

4. Center for Theoretical Biological Physics, Rice University, Houston, TX 77005, USA.

5. Department of Chemistry, Massachusetts Institute of Technology, Cambridge, MA 02139, USA.

6. Department of Pathology and Immunology, Baylor College of Medicine, Houston TX 77030, USA.

7. Center for Drug Discovery, Baylor College of Medicine, Houston TX 77030, USA.

8. Department of Molecular and Human Genetics, Baylor College of Medicine, Houston TX 77030, USA.

9. Huffington Center on Aging, Baylor College of Medicine, Houston, TX 77030, USA.

10. Howard Hughes Medical Institute, Baylor College of Medicine, Houston, TX 77030, USA.

11. Department of Internal Medicine, Division of Hematology, The Ohio State University, Columbus, OH 43210.

12. Department of Molecular and Cellular Biology, Baylor College of Medicine, Houston TX 77030, USA.

† Contributed equally

* Corresponding email: wangj@bcm.edu

Abstract

Current efforts in the proteolysis targeting chimera (PROTAC) field mostly focus on choosing an appropriate E3 ligase for the target protein, improving the binding affinities towards the target protein and the E3 ligase, and optimizing the PROTAC linker. However, due to the large molecular weights of PROTACs, their cellular uptake remains an issue. Through comparing how different warhead chemistry, reversible noncovalent (RNC), reversible covalent (RC), and irreversible covalent (IRC) binders, affects the degradation of Bruton's Tyrosine Kinase (BTK), we serendipitously discovered that cyano-acrylamide-based reversible covalent chemistry can significantly enhance the intracellular accumulation and target engagement of PROTACs and developed RC-1 as the first reversible covalent BTK PROTAC with a high target occupancy as its corresponding kinase inhibitor and effectiveness as a dual functional inhibitor/degrader, a novel mechanism-of-action for PROTACs. Importantly, this reversible covalent strategy is generalizable to improve other PROTACs, opening a new path to enhance PROTAC efficacy.

Introduction

A proteolysis targeting chimera (PROTAC) is a heterobifunctional molecule that can bind both a target protein and an E3 ubiquitin ligase to facilitate the formation of a ternary complex, leading to ubiquitination and ultimate degradation of the target protein [1]. Since Crews and Deshaies conceived the PROTAC concept in 2001 [2], PROTACs have gained tremendous attention in recent years not only for their numerous applications in chemical biology but also as highly promising therapeutic agents [1]. Compared with oligonucleotide and CRISPR therapeutics that face *in vivo* delivery challenges, PROTACs are small molecule therapeutics that provide opportunities to achieve broadly applicable body-wide protein knockdown. ARV-110, an oral androgen receptor (AR) protein degrader, is the first PROTAC hitting the clinic in 2019 [3].

Protein degraders have many advantages compared with traditional small molecule inhibitors. First, small molecule inhibitors usually modulate protein functions through stoichiometrically occupying the active sites or binding pockets of targeted proteins; however, PROTACs act as catalysts and are involved in multiple cycles of targeted protein degradation [4, 5]. Therefore, the degradation induced by PROTACs is sub-stoichiometric. Second, due to the competitive nature of small molecule inhibitors, constant systemic drug exposure is necessary to maintain sufficient intracellular concentrations for therapeutic efficacy, usually leading to off-target and side effects. In contrast, optimized PROTACs usually achieve maximal protein degradation in a few hours and maintain the therapeutic effect (even without constant PROTAC exposure) until the targeted protein is re-synthesized in cells. Therefore, the pharmacodynamics (PD) of PROTACs is dependent on not only drug exposure (pharmacokinetic (PK) properties) but also the half-life ($t_{1/2}$) of the targeted protein. Third, small molecules usually interfere with the function of one domain of a multidomain protein. However, this strategy for multidomain kinases, especially in cancer cells, may lead to compensatory feedback activation of its downstream signaling pathways *via* other alternative kinases [6]. In contrast, although PROTACs only target one domain of a multidomain protein, they induce degradation of the full-length protein, reducing the possibility to develop drug resistance through mutations or compensatory protein overexpression and accumulation [7]. Fourth, the specificity of small molecule inhibitors depends solely on the molecular design, which is sometimes difficult to achieve due to the presence of proteins with similar binding pockets, such as kinases. In contrast, the specificity of PROTACs is determined by not only the small molecule binder to targeted proteins but also the protein-protein interactions between the targeted protein and the recruited E3 ligase [8, 9, 10, 11]. Last but not least, the targets of small molecular

inhibitors are usually enzymes and receptors with defined binding pockets or active sites. However, ~75% of the human proteome lacks active sites, such as transcription factors and non-enzymatic proteins, and are considered 'undruggable' [1]. In contrast, PROTACs can be designed to bind to any crevice on the surface of the targeted proteins to induce their degradation [12].

Most PROTACs reported thus far have been based on noncovalent binding to their target proteins. Although irreversible covalent inhibitors, such as ibrutinib, have achieved tremendous clinical success based on their strong target affinities and high target occupancies, it was recently reported that PROTACs with irreversible covalent binders to targeted proteins failed to induce efficient protein degradation [13]. Although the potential mechanism accounting for the inhibition of protein degradation was not elucidated, it was postulated that irreversible covalent PROTACs are unable to induce protein degradation in a sub-stoichiometric/catalytic manner because they are consumed once they bind to their targeted protein. However, there are also examples arguing against this hypothesis [5, 14].

Reversible covalent chemistry previously enabled our development of a series of fluorescent probes that can quantify glutathione concentrations in living cells [15, 16, 17, 18, 19]. We were curious whether reversible covalent PROTACs can not only enhance the binding affinity to targeted protein but also overcome the "one-shot deal" drawback of irreversible covalent PROTACs (**Figure 1**). Beginning as a basic science exploration to compare how the warhead chemistry of PROTACs with reversible noncovalent (RNC), reversible covalent (RC), and irreversible covalent (IRC) binders affect protein degradation, we chose Bruton's tyrosine kinase (BTK) as a model target to test the hypothesis. To our surprise, we discovered that cyano-acrylamide-based reversible covalent binder to BTK can significantly enhance drug accumulation and target engagement in cells. Building on this discovery, we developed RC-1 as the first reversible covalent BTK PROTAC with a high target occupancy as its corresponding kinase inhibitor. RC-1 is effective as a dual functional inhibitor/degrader, providing a novel mechanism-of-action for PROTACs, and forms a stable ternary complex by reducing protein conformational flexibility compared with the non-covalent PRTOAC counterparts. Importantly, we found that this reversible covalent strategy can be generalized and applied to improve other PROTACs. We hope that this study adds another dimension to improve the cellular efficacy of PROTACs.

Results

Comparison of Different PROTAC Warhead Chemistry for BTK Degradation

As the first FDA-approved covalent kinase inhibitor, Ibrutinib irreversibly reacts with the free cysteine residue (C481) in the active site of BTK to form a covalent bond. It is also known that ibrutinib can still bind to the C481S BTK mutant mostly through hydrogen bonding, but with >40 folds lower affinity [20]. Johnson et al. showed that ibrutinib is >6 folds more potent than its Michael acceptor saturated ibrutinib analog in a kinase inhibition assay for wild type BTK (IC_{50} 0.72 nM vs 4.9 nM), while both compounds are equally potent towards BTK C481S mutant (IC_{50} 4.6 nM vs 4.7 nM) [21]. To compare how different warhead chemistry may affect the target protein degradation, we designed three PROTAC molecules, RC-1, RNC-1 and IRC-1, which form reversible covalent (RC), reversible noncovalent (RNC), and irreversible covalent (IRC) binding to BTK (**Figure 2A**). Following previous work [13, 22, 23, 24, 25, 26], we chose pomalidomide as the CRBN E3 ligase binder. RC-1, RNC-1 and IRC-1 share the same linker and E3 ligand binder and differ only by the binding moieties to BTK. We chose MOLM-14, an acute myeloid leukemia cell line, as a model system to study PROTAC-mediated BTK degradation following previous work [23].

To test whether the three PROTACs can induce BTK degradation, we treated MOLM-14 cells with RC-1, RNC-1 and IRC-1 for 24 h, followed by Western blot to quantify the total BTK levels (**Figure 2B**). Consistent with Tinworth et al.'s recent report [13], IRC-1 induced inefficient BTK degradation. Comparing RC-1 and RNC-1, we found that RC-1 was more potent for BTK degradation than RNC-1 at lower concentrations (8 and 40 nM) and comparable to RNC-1 at 200 nM. RC-1 potently induced BTK degradation in MOLM-14 cells (DC_{50} = 6.6 nM, **Figure 2C**), as one of the most potent BTK degraders reported so far [13, 24]. Additionally, neither the RC-1 warhead, nor pomalidomide, nor a combination of both caused BTK degradation (**Figure 2D**), indicating that the bifunctional PROTAC molecule is essential to facilitate the formation of a ternary complex of {BTK-PROTAC-CRBN} to induce BTK degradation.

Linker Optimization for Reversible Covalent BTK PROTAC

Encouraged by the promising result for RC-1, we set out to optimize the linker between the BTK covalent reversible binder and pomalidomide (**Figure 3**). In a recent study from Pfizer, Zorba et al. showed that increasing PROTAC linker length alleviates steric clashes between BTK and CRBN and improves the efficacy of BTK degradation [24], indicating the absence of thermodynamic cooperativity in the formation of a ternary complex of

{BTK-PROTAC-CRBN}. Therefore, we synthesized RC-2, RC-3, RC-4 and RC-5, which are 1, 2, 5, and 8 atoms longer in the linker length compared with RC-1. Contrary to Pfizer's finding, we found that RC-1 is the most efficacious for BTK degradation compared with the PROTACs possessing longer linkers, suggesting cooperative ternary complex formation (**Supplementary Figure 1**).

To test whether the BTK degradation efficacy of RC-1 can be improved through further reducing the linker length, we designed RC-6, RC-7 and RC-8, which are 1, 2, and 3 atoms shorter in the linker length compared with RC-1. Unfortunately, we could not synthesize RC-6 due to an intramolecular reaction between the amide and the Michael acceptor. Comparing the BTK degradation capability in MOLM-14 cells, we found that RC-7 and RC-8 are inferior to RC-1, possibly due to unfavorable steric clashes between BTK and CRBN. We also found that the efficacy of BTK degradation decreases significantly through only a single atom change of the thalidomide aryl amine nitrogen to an oxygen (RC-9) (**Supplementary Figure 1**).

In Buhimschi et al.'s recent study, a BTK PROTAC MT-802 has the linker placed at the C5 position on the phthalimide ring of pomalidomide instead of the C4 position as in RC-1. We synthesized RC-10 by placing the linker at the C5 position of the phthalimide ring and found that RC-10 cannot induce any BTK degradation (**Supplementary Figure 1**). Therefore, we concluded that RC-1 has the optimal linker length and position for BTK degradation with the BTK and CRBN binders used.

Quantitative Measurements of BTK and CRBN Concentrations in Cells

The Crews group developed a series of PROTACs for TANK-Binding Kinase 1 (TBK-1) with different binding affinities towards TBK-1 and von Hippel-Lindau (VHL), the E3 ligase recruited [27]. We re-analyzed the data in this study and found a strong correlation between binding affinities towards TBK-1 and the DC_{50} values in cells (**Supplementary Figure 2**), suggesting that tighter binding to the target protein leads to more efficient PROTAC-induced protein degradation in cells. In our study, it is reasonable to assume that the binding affinity of RC-1 to BTK is higher than RNC-1 due to the covalent bond formed between RC-1 and BTK. It could be taken for granted that tighter binding to BTK leads to more formation of the ternary complex, resulting in more efficient BTK degradation. However, the formation of the {BTK-PROTAC-CRBN} ternary complex depends on not only the binding affinities of PROTAC towards BTK and CRBN but also the **absolute concentrations** of BTK, CRBN and PROTAC in cells. To the best of our knowledge, previous studies on PROTACs only focus on the biochemical

measurements for binding affinities of PROTACs to target proteins and E3 ligases without knowing the intracellular concentrations of these proteins.

We performed quantitative Western blots to measure the levels of BTK and CRBN in MOLM-14 cells using a series of concentrations of their corresponding recombinant proteins as the standards. Lysate from a million MOLM-14 cells usually produces 250 μg of protein as determined by BCA assays. Because proteins usually occupy 20-30% of cell volume (assuming 25% w/v, i.e., 250 mg/mL) [28], we can calculate the volume of 1 million MOLM-14 cells to be ~1 μL (i.e., the volume of each MOLM-14 cell is ~1000 μm^3). Based on quantitative Western blots, we determined the total amount of BTK and CRBN in 1 million MOLM-14 cells to be 60 and 0.72 ng, respectively. Considering the molecular weights of BTK and CRBN are 77 kD and 55 kD, we can deduce the absolute concentrations for BTK and CRBN in MOLM-14 cells are 780 and 13 nM, respectively (**Figure 4A and Supplementary Figure 3**). Based on our biochemical binding assays, the *K*d values between PROTACs and BTK are in the range of 3.0–6.4 nM (**Table 1**), while the *K*d values between the PROTACs and CRBN are in the range of 1.5–4.2 μM (**Table 2**). Assuming there is no cooperativity effect in the formation of the ternary complex {BTK-PROTAC-CRBN}, we can predict that BTK PROTACs binding to CRBN is the determining factor for ternary complex formation due to the low abundance of CRBN and the weak binding between pomalidomide and CRBN. Therefore, under this situation, further increasing PROTAC binding affinities to BTK, such as comparing RC-1 and RNC-1, would not lead to a meaningful increase of ternary complex formation. This conclusion is also supported by the mathematical model for three-body binding equilibria developed by Douglass et al. [29] (**Supplementary Figure 4**).

Fluorophore Phase Transition-Based Imaging of Ternary Complex Formation in Live Cells

To visualize small molecule-induced protein-protein interactions (PPIs), we recently applied fluorophore phase transition-based principle and designed a PPI assay named SPPIER (separation of phases-based protein interaction reporter) [30]. A SPPIER protein design includes three domains, a protein-of-interest, an enhanced GFP (EGFP) and a homo-oligomeric tag (HOTag). Upon small molecule-induced PPI between two proteins-of-interest, multivalent PPIs from HOTags drive EGFP phase separation, forming brightly fluorescent droplets [30]. Here, to detect PROTAC-induced PPI between BTK and CRBN, we engineered the kinase domain of BTK (amino acid residues 382 – 659, referred to as BTK^{KD}) into SPPIER to produce a BTK^{KD}-EGFP-HOTag6 construct, which

forms tetramers when expressing in cells (**Figure 5A**). The previously reported CRBN-EGFP-HOTag3 fusion construct [30], which forms hexamers in cells, was used as the E3 ligase SPPIER (**Figure 5A**). If PROTACs can induce {BTK-PROTAC-CRBN} ternary complex formation in cells, they will crosslink the BTK^{KD}-EGFP-HOTag6 tetramers and the CRBN-EGFP-HOTag3 hexamers to produce EGFP phase separation, which can be conveniently visualized with a fluorescence microscope. This assay is named as BTK-SPPIER. HEK293 T/17 cells were transiently transfected with both constructs. Twenty-four hours after transfection, the cells were incubated with 10 μM of RC-1, IRC-1 or RNC-1. Live cell fluorescence imaging revealed that RC-1, but not IRC-1 nor RNC-1, induced appreciable green fluorescent droplets (**Figure 5B**). This imaging result indicated that RC-1 is more efficient to induce {BTK-PROTAC-CRBN} ternary complex formation in living cells than RNC-1 and IRC-1 under the same experimental conditions. It should be noted that the concentration needed for RC-1 to induce appreciable droplet formation in this assay is much higher than its DC_{50} in MOLM-14 cells potentially due to the high overexpression of the target proteins and the sensitivities of the assay.

Inhibition of Cell Viabilities by BTK Degraders

We next examined the potencies of inhibiting cell growth for RC-1, IRC-1, RNC-1, RC-1-Me (RC-1 non-degrader control), and their corresponding BTK binder controls, RC-Ctrl, IRC-Ctrl (i.e. ibrutinib), and RNC-Ctrl in MOLM-14 cells. All the chemical structures and IC_{50} values can be found in **Figure 2A** and **Table 1,** respectively. Differing by a methyl group, RC-1 can but RC-1-Me cannot degrade BTK in cells (**Figure 2D**). Interestingly, both compounds have similar IC_{50} values (0.31 vs 0.21 μM), suggesting that BTK inhibition but not degradation accounts for the toxicity in MOLM-14 cells. The IC_{50} values for RC-Ctrl, IRC-Ctrl, and RNC-Ctrl are also similar in the range of 0.3–0.5 μM, suggesting that these three warheads inhibit BTK to a similar extent in cells. Surprisingly, both the IC_{50} values for IRC-1 and RNC-1 are in the μM range (2.7 and 4.1 μM). A biochemical BTK kinase inhibition assay showed that IRC-1 and RNC-1 have slightly diminished inhibitory activities (< 3-fold) compared with their corresponding warhead controls (**Table 1**). However, the difference between enzymatic activities is insufficient to explain the >10-fold difference in IC_{50} values in cells, suggesting that IRC-1 and RNC-1 may have poorer intracellular accumulation than their corresponding warhead controls. In contrast, RC-1 and RC-Ctrl have similar IC_{50} values in both biochemical BTK inhibition and cellular growth inhibition assays (**Table 1**), suggesting similar compound exposure in cells. The growth inhibition assay for the BTK degraders prompted us to investigate alternative mechanisms to explain the high potency of RC-1.

Comparison of Intracellular Concentrations of BTK Degraders

Since the binding affinities between BTK and its PROTACs cannot explain the difference in BTK degradation between RC-1 and RNC-1 and potencies for cell growth inhibition among RC-1, RNC-1 and IRC-1, we asked whether the intracellular concentration of RC-1 may be higher than those of RNC-1 and IRC-1, leading to more potent pharmacological effects. To test this possibility, we turned to the Nano-luciferase based bioluminescence resonance energy transfer (NanoBRET) assay developed by Promega [31]. HEK-293 cells were transiently transfected with plasmids expressing a fusion protein of Cereblon and nano-luciferase (nLuc) for 24 h and then the cells were treated with a Cereblon tracer, which binds to Cereblon to induce NanoBRET signals. Adding PROTACs to cells would compete the CRBN tracer binding to CRBN, thus reducing the NanoBRET signals. The target engagement IC_{50} is defined as the concentration of an unlabeled compound that results in a half-maximal inhibition binding between the fluorescent tracer and the nanoLuc fusion protein [32]. It should be noted that the NanoBRET assay is ratiometric and independent of the expression level of the nanoLuc fusion protein. Based on this assay, we found that the CRBN target engagement IC_{50} value of RC-1 is 3 and 7-fold as low as those of IRC-1 and RNC-1, respectively (**Figure 4B**). It should be noted that target engagement IC_{50} values are dependent on assay conditions, including the tracer concentration and the expression level of the nanoLuc fusion protein. Therefore, the target engagement IC_{50} values for different compounds can only be meaningfully compared under the same assay conditions.

To quantitatively compare the intracellular concentrations of these PROTACs, we defined a parameter $K_{P,D}$ as the intracellular accumulation coefficient for drug D, in which P and D denote partition and drug, respectively, following the previous work [33]. $K_{P,D}$ is defined as the ratio between the total intracellular and extracellular concentrations of drug D and calculated as $K_{P,D} = \frac{C_{D,in}}{C_{D,ex}}$, where $C_{D,in}$ and $C_{D,ex}$ are the total intracellular and extracellular concentrations of drug D, respectively. When 50% of target engagement is reached with the addition of drug D to the medium (i.e. $C_{D,ex} = IC_{50,TE}$ assuming intracellular drug accumulation does not significantly change the extracellular drug concentration; $C_{D,in} = [D]$ assuming the total intracellular concentration of drug D is much greater than that of the target protein P), we can deduce that $K_{P,D} = \frac{C_{D,in}}{C_{D,ex}} = \frac{[D]}{IC_{50,TE}} = \frac{K_{d,D}}{IC_{50,TE}}\frac{[PD]}{[P]}$, where $K_{d,D}$ is the dissociation equilibrium constant for the binding between the target protein or its nanoLuc fusion and the drug, [P] is the equilibrium concentration of the target protein nanoLuc fusion, [D] is the equilibrium

concentration of the free drug D, [PD] is the equilibrium concentration of the drug bound form of the target protein nanoLuc fusion, and $IC_{50,TE}$ is the target engagement IC_{50} in the NanoBRET assay. Under the same assay conditions, [PD] and [P] are constants and [PD]/[P] can be defined as a constant A. So, we can deduce that $K_{P,D} = A\frac{K_{d,D}}{IC_{50,TE}}$. We further define the relative intracellular accumulation coefficient for drug D ($K'_{P,D}$) as $K'_{P,D} = \frac{K_{P,D}}{A} = \frac{K_{d,D}}{IC_{50,TE}}$. Under the same assay conditions, a greater $K'_{P,D}$ value for a drug reflects its higher tendency to accumulate inside cells. It should be noted that $K_{P,D}$ is independent of assays and assay conditions but requires quantification of [P] and [PD]. In contrast, $K'_{P,D}$ is an assay condition dependent parameter but provides a convenient approach to quantitatively compare the tendency of intracellular accumulation of drugs.

Based on the $K'_{P,D}$ values calculated by dividing the K_d to CRBN with the in-cell target engagement IC_{50} (**Table 2**), we can deduce that the intracellular concentration of RC-1 is 10 and 16-fold as the levels of IRC-1 and RNC-1, respectively. Additionally, the calculated CLogP and polar surface area (PSA) values for these three compounds are similar (**Supplementary Table 1**), arguing against the possibility that the physicochemical properties of RC-1 are the cause of its high intracellular concentration. Therefore, we conclude that the efficient BTK degradation and potent cell growth inhibition induced by RC-1 is achieved mostly through its high intracellular concentration, due to the reversible covalent structural moiety in RC-1.

RC-1 is a unique BTK degrader with high target occupancy

Although the PROTACs are characterized as BTK degraders, they have warheads that can bind and inhibit BTK, essentially as dual-functional BTK inhibitors and degraders. We performed biochemical BTK kinase inhibition assays to measure the IC_{50} values for RC-1, RNC-1 and IRC-1 and their corresponding warhead controls (**Table 1** and **Supplementary Figure 5**). IRC-Ctrl (i.e. Ibrutinib) forms a covalent bond with BTK and is expected to be the most potent BTK inhibitor (IC_{50} = 0.3 nM). In comparison, RC-Ctrl and RNC-Ctrl have reduced BTK inhibition activities by 7 and 45 folds, respectively. The BTK PROTACs, RC-1, RNC-1, and IRC-1, have similar BTK inhibitory activities to their corresponding warheads (**Table 1 and Supplementary Figure 5**).

We then performed a similar NanoBRET based live-cell target engagement assay for BTK. Consistent with the CRBN target engagement assay, we found that the BTK target engagement IC_{50} value of RC-1 is 3 and 30 folds of the values for IRC-1 and RNC-1, respectively (**Figure 4C**). Based on the $K'_{P,D}$ values calculated by

dividing the K_d to BTK with the in-cell target engagement IC_{50} (**Table 1**), we can deduce that the intracellular concentration of RC-1 is 6 and 40 folds as high as those of IRC-1 and RNC-1, respectively, similar to the trend observed in the CRBN target engagement assay (**Figure 4B**).

To further rule out the possibility that the enhanced intracellular accumulation and target engagement of RC-1 is due to its physical properties, we synthesized two additional control compounds RNC-1-CN-DiMe and IRC-1-DiMe (**Supplementary Figure 6**). RNC-1-CN-DiMe can be viewed as direct reduction of the C=C double bond in the Michael acceptor of RC-1 to a single bond. IRC-1-DiMe can be viewed as RC-1 only lacking the cyano group but maintaining the dimethyl moiety. The BTK target engagement IC_{50} value of RC-1 is at least an order of magnitude smaller than the values for IRC-1-DiMe and RNC-1-CN-DiMe, respectively (**Table 1 and Supplementary Figure 6**). Calculating the $K'_{P,D}$ values, we can deduce that the intracellular concentration of RC-1 is 5 folds of those of IRC-1-DiMe and RNC-1-CN-DiMe (**Table 1**), arguing against that the enhanced intracellular accumulation of RC-1 is attributed to the physical property changes caused by the additional cyano or dimethyl groups in RC-1 compared with IRC-1 and RNC-1.

Due to poor intracellular accumulation, most PROTACs have low target occupancy (**Figure 4D**) and rely on the sub-stoichiometric protein degradation to achieve maximal efficacy. Using the NanoBRET-based BTK in-cell target engagement assay, we found that RC-1 can achieve 50% and 90% of target engagements at 40 and 200 nM, respectively. Therefore, RC-1 can function as both a BTK inhibitor and degrader.

RC-1 degrades BTK regardless of its mutation status

Mutations in BTK, C481S in particular, confer ibrutinib resistance in clinic [20]. We set out to test whether BTK degradation induced by our PROTACs is affected by BTK mutation status. XLA cells overexpressing wild type BTK or C481S mutant BTK were treated with RC-1, RNC-1 and IRC-1 for 24 h, followed by Western blot to compare the BTK levels (**Figure 6A and Supplementary Figure 7**). We observed dose-dependent BTK degradation induced by RC-1 regardless of its mutation status with comparable potency. This observation is consistent with our previous conclusion that altering PROTAC binding affinities to BTK within a range does not significantly change the ternary complex formation efficiency (**Supplementary Figure 4**). It should be noted that the potency of RC-1 is weaker in XLA cells than in MOLM-14 cells possibly because BTK is overexpressed in XLA cells. It is also interesting to note that IRC-1 induces much more effective degradation of the BTK C481S

mutant than its wild type in XLA cells (**Supplementary Figure 7**), suggesting that the irreversible covalent bond formation between IRC-1 and BTK causes the inefficient protein degradation, consistent with the previous study by the GSK group [13].

RC-1 degrades BTK with higher specificity than IRC-1 and RNC-1

To explore the effects of our degraders on the whole proteome, we treated MOLM-14 cells with RC-1, RNC-1, IRC-1, RC-1-Me (non-degrader control) or DMSO and employed a quantitative multiplexed proteomic approach to measure the whole cellular protein levels (**Figure 7**). The result showed that both in IRC-1 and RNC-1-treated cells, 7 kinases are degraded including BTK. However, for RC-1-treated cells, only 2 kinases (BTK and CSK) can be degraded, suggesting that RC-1 has more selectivity than IRC-1 and RNC-1 for kinase degradation. However, no degradation is observed in RC-1-Me-treated cells, indicating that the degradation observed for RC-1 is CRBN dependent. In addition, immunomodulatory imide drugs (IMiD)-dependent substrates including IKZF1, ZFP91 and ZNF692 are also specifically degraded by RC-1, RNC-1 and IRC-1.

Molecular dynamics simulations predict a stable ternary complex for RC-1

To better understand the ternary complex formation, we applied molecular dynamics simulations to evaluate the global rearrangement of the ternary structures for BTK, CRBN, and RC-1 or IRC-1 or RNC-1, and compared the binding stabilities of these three ligands to BTK and CRBN. The residue-based RMSF (root mean square fluctuations) was calculated based on the entire simulation trajectory (>200 ns) to assess the average fluctuation of each residue of the three simulated complexes. It is clear that RNC-1 mediated complex {BTK-RNC-1-CRBN} has the largest fluctuation compared with the other two complexes {BTK-RC-1-CRBN} and {BTK-IRC-1-CRBN} (**Figure 8A**), suggesting that covalent binding could help to overcome the unfavorable entropy penalties during the ternary complex formation. Additionally, the RMSD (Root-mean-square deviation) values were calculated based on the Cα atoms to reflect the conformation changes from the input structures based on x-ray crystallography. Consistent with the RMSF analyses, the RMSD changes for the {BTK-RC-1-CRBN} and {BTK-IRC-1-CRBN} complexes are much smaller than the one for the {BTK-RNC-1-CRBN} complex, suggesting that covalent bonding can help to stabilize the ternary complexes (**Figure 8B**).

Low energy conformations of the protein complex can shed light on the detailed molecular interactions which stabilize the binding interface. The conformation with the lowest energy along the trajectories was extracted and

shown in **Figure 8C**. The binding mode and critical molecular interactions, i.e., hydrogen bonds and π-π interactions formed between the ligands and BTK and CRBN, are conserved compared to the crystal structure of BTK/ibrutinib and CRBN/lenalidomide. From the predicted binding mode, several hydrogen bonds and the covalent bond between RC-1 and the residue C481 of BTK anchors the ligand to the binding site of BTK. Additionally, a hydrogen bond between Y355 of CRBN and anion-π interaction formed between H353, hence, further greatly stabilizes the binding of RC-1 with proteins, and help to hold the orientation of RC-1 to adjust and stabilize the ternary complexes (**Figure 8C**).

RC-1 outperforms other reported BTK degraders in cell viability and target engagement assays

The goal of blocking BTK signaling with either BTK inhibitors or degraders is to inhibit the growth of cancer cells. To this end, we synthesized previously reported BTK degraders DD-03-171 [26] and MT-802 [25] and compared them head-to-head with RC-1, RNC-1 and IRC-1 in their abilities to inhibit cancer cell growth (**Figure 9 and Supplementary Figure 8**). Due to the structural similarities of RNC-1 and the BTK degraders reported by the GSK group (PROTAC 5) [13] and the Rao group [22], we used RNC-1 as a surrogate for comparison. In MOLM-14 cells, RC-1 has the most potent inhibitory effect among all the PROTACs compared (**Figure 9 and Supplementary Figure 8**). It is interesting to note that RC-1 and RC-1-Me, which does not induce BTK degradation, have similar IC_{50} values in inhibiting MOLM-14 cell growth, indicating that the growth inhibitory effect induced by PROTACs in MOLM-14 cells is due to BTK inhibition instead of its degradation. The high potency of RC-1 is possibly due to the combinatorial effects of its high intracellular concentration and tight binding to BTK.

We also compared the potency of BTK degraders in Mino cells, a BTK dependent MCL cell line. In Mino cells, RC-1 and DD-03-171 have comparable potency for inhibiting cell growth and outperform all the other BTK PROTACs tested (**Figure 9**). Additionally, RC-1 can degrade not only BTK and phosphorylated BTK but also IKZF1 and IKZF3 (**Figure 6B**), similar to DD-03-171 [26]. It is interesting to note that RC-1 is more potent than ibrutinib in Mino cells, but have similar potencies in Jeko-1, Rec-1 and Maver-1 cells (**Supplementary Table 2**). Further investigation is required to identify biomarkers for the subtype of MCL sensitive to BTK degraders.

Additionally, we compared BTK in-cell target engagement among RC-1, RC-Ctrl (RC-1 warhead) and these reported BTK degraders (**Figure 4D**). It is remarkable to see that the target engagement IC_{50} values for RC-1

and RC-Ctrl (59 vs 47 nM) are the same within experimental errors, demonstrating that the intracellular accumulation of RC-1 is essentially the same as its parent warhead molecule although their molecular weights differ by 1.7 folds. In contrast, the target engagement IC_{50} values for DD-03-171 and MT-802 are 5 and 11 folds as high as of that of RC-1, respectively.

RC-1 has an ideal plasma half-life and degrades BTK in vivo

We measured the plasma half-life of RC-1 (20 mg/kg, i.p. injection) in ICR mice (female, 5-6 weeks, n=3) using LC-MS/MS. The PK data were fitted into a non-compartmental model using PK solver [34]. RC-1 has a plasma half-life ($t_{1/2}$) of 3.4 h, C_{max} of 20 μM, and AUC of 72 μM·h (**Figure 10A**). To further test the pharmacodynamics of RC-1 *in vivo*, we treated ICR mice (n=3) with 20 mg/kg of RC-1 (i.p. injection). After 7 days injection, the mice were sacrificed, and their spleens, the locations of the majority of B cells, were collected. Western blotting showed that RC-1-treated mice had ~50% BTK level reduction in the spleens compared with the vehicle-treated mice (**Figure 10B**). Therefore, this preliminary study showed that RC-1 has desirable PK/PD properties *in vivo*, laying the foundation for future efficacy tests in mouse models to ultimately move this degrader into the clinic.

Other reversible covalent PROTACs with improved target engagement

Based on the success of RC-1, we were curious whether cyano-acrylamide based reversible covalent PROTACs can be generally applied to improve target engagement. An activating mutation of Fms-like tyrosine kinase 3 (FLT3) is the most frequent genetic alteration associated with poor prognosis in acute myeloid leukemia (AML). Similar to BTK, FLT3 also has a cysteine residue in the ATP binding pocket. Yamaura et al. reported a highly potent irreversible covalent FLT3 inhibitor, termed as FF-10101 [35]. Building on this work, we designed a series of reversible covalent, irreversible covalent and reversible non-covalent FLT3 PROTACs. Using the NanoBRET CRBN in-cell target engagement assay, we found that RC-FLT3 has a similar target engagement IC_{50} value compared with that for pomalidomide (**Figure 11**). Similar to BTK PROTACs, the target engagement IC_{50} values for IRC-FLT3 and RNC-FLT3 PROTACs are 5 and 34 folds as high as that for RC-FLT3 (**Figure 11**). This experiment confirmed that introducing a cyano-acrylamide moiety can be a general strategy to enhance intracellular accumulation and target engagement for PROTACs.

Discussion

Despite the exciting promise of PROTACs, the development of this type of therapeutic agent faces some major challenges. Due to the high molecular weights of PROTACs, they are not druglike based on the commonly applied empirical rules for drug discovery and tend to have poor membrane permeabilities, resulting in low drug concentrations inside cells. Therefore, PROTACs usually have low target occupancy and heavily depend on sub-stoichiometric protein degradation to achieve therapeutic efficacy. Although there are successful PROTAC examples with potent *in vitro* and *in vivo* efficacies, they are mostly optimized through "brute force" medicinal chemistry efforts. To the best of our knowledge, few efforts have been focused on developing general strategies to improve the intracellular accumulation of PROTACs.

In this work, we serendipitously discovered that cyano-acrylamide groups can enhance intracellular accumulation of PROTACs. We prefer the term "enhanced intracellular accumulation" instead of "enhanced permeability" to describe the unique feature of RC-1. Permeability characterizes the potential for a compound to transverse the plasma membrane of cells, which can be energy independent or dependent. In contrast, intracellular accumulation is a general term to describe the extent of an exogenous compound remains inside cells, which is an agglomerate effect determined by permeability, specific and non-specific interactions with intracellular proteins and other biomolecules, and elimination through metabolism and drug efflux pumps.

Based on Taunton's and our own previous work [16, 19, 36], it has been well established that cyano-acrylamides can reversibly react with thiols with mM dissociation equilibrium constants (K_d). Additionally, the reaction kinetics between cyano-acrylamides and free thiols are fairly rapid. During the development of our GSH probes, we found that the RealThiol probe can establish equilibrium with GSH in 90 seconds in both forward and reverse reactions. It is possible that the enhanced intracellular accumulation of RC-1 is due to its fast and reversible reactions with intracellular glutathione (usually in the range of 1-10 mM), serving as a sink to trap RC-1 in cells. In contrast, RNC-1 cannot react with GSH. Technically, IRC-1 can irreversibly react with GSH but with a much slower reaction rate. This hypothesis could be tested by measuring the target engagement IC_{50} values of RC-1 at different intracellular GSH concentrations in HEK293 cells. Additionally, it is also possible that many available free cysteine residuals on the cellular surface can reversibly react with cyano-acrylamide containing molecules to mediate the enhanced cellular uptake. The Matile group reported that strained cyclic disulfides can enhance cellular uptake of non-permeable molecules through a similar mechanism [37, 38]. Although understanding the

molecular mechanism of enhanced intracellular accumulation of RC-1 is out of the scope of this work, it would be interesting to explore other reversible covalent chemistry to enhance the cellular uptake of poorly permeable molecules.

We attempted to measure the permeabilities of RC-1, IRC-1 and RNC-1 using the lipid-PAMPA method (**Supplementary Table 3**). Unfortunately, none of the compounds were detected on the receptor side, indicating extremely poor physical permeabilities. Additionally, the total recovery rates for all the three compounds were only in the range of 20-30%, suggesting that these compounds may stick to the PAMPA lipids and/or the plasticware used in this assay. Therefore, we concluded that the lipid-PAMPA method is not an ideal assay to evaluate the permeabilities of our PROTACs.

We developed the concept of relative intracellular accumulation coefficient $K'_{P,D}$ to quantitatively compare the intracellular concentrations of drugs under the same assay conditions, taking advantage of the live-cell based NanoBRET assays. Initially, we attempted to use LC-MS to quantify the intracellular concentrations of the PROTACs by extracting them from the cell lysates (**Supplementary Table 4**). Although we found that RC-1 has slightly higher concentrations (~ 2-fold) than RNC-1 and IRC-1 inside cells, it is difficult to differentiate whether the drug molecules measured are indeed intracellular or non-specifically attach to the cell surface using the lysate method. Considering the “greasy” nature of the PROTACs revealed in the lipid-PAMPA permeability experiment, we are concerned about the accuracy of the lysate-based drug quantification in cells. In contrast, the live cell-based NanoBRET assays are less prone to the artefacts associated with lysate-based methods and produce more reliable comparison of target engagement and intracellular concentration of PROTACs. Combining the target engagement IC_{50} values in the NanoBRET assays and the dissociation equilibrium constants (K_d) between the drug and the target protein, we can calculate the relative intracellular accumulation coefficient $K'_{P,D}$ as a convenient and reliable method to compare the tendency of drugs accumulating in cells.

Despite RC-1 is highly potent to degrade BTK in human cell culture and has a favorable PK property in mice, maintaining the plasma concentration above 200 nM over 24 h with a single i.p. injection of RC-1 (20 mg/kg), it is interesting to note that the maximum BTK degradation achieved in spleenic B cells in mice is only ~50% even with 7 daily injections. To reconcile the discrepancy, we treated a mouse B cell lymphoma cell line derived from Eu-Myc mice with RC-1 *in vitro* and found that the maximum BTK degradation is only 30-40% even dosed up to 25 μM of RC-1 (**Supplementary Figure 10**), indicating that RC-1 is indeed much less potent for BTK degradation

in mouse cells than in human cells. Although thalidomide and its derivatives, lenalidomide and pomalidomide, are clinically effective treatments for multiple myeloma, they are inactive in murine models *in vivo* due to the sequence differences between mouse and human Cereblon [39, 40]. Mice with a single I391V amino acid change in Crbn restored thalidomide-induced degradation of drug targets previously found in human cells [39, 40]. We rationalize that the BTK degradation potency difference for RC-1 in human and mouse cells may be due to the sequence variations for BTK and/or CRBN in different species, leading to inefficient formation of the ternary complex among RC-1, mouse Btk and mouse Crbn due to altered protein-protein interactions. This raised a question whether mice with humanized CRBN, either I391V and/or other mutations, should be developed to properly access the efficacy and toxicity of CRBN recruiting PROTACs in murine models, which can be a future research direction.

The efficacy of irreversible covalent PROTACs has been controversial, with both successful [5, 14] and unsuccessful examples [13]. An apparent drawback for irreversible covalent PROTACs is its non-catalytic degradation of target proteins. If we examine the target engagement data for IRC-1 (**Figure 4B and 4C**), it can achieve ~100% BTK and ~40% CRBN engagement at 400 nM of IRC-1. Assuming the target engagement IC_{50} values are similar in the HEK293 over-expression system and MOLM-14 cells, we would expect to observe significant BTK degradation with 400 nM of IRC-1 treatment, even with the single turnover degradation. However, very little BTK degradation was observed in MOLM-14 cells with IRC-1 treatment, suggesting either BTK was not efficiently ubiquitinated due to the poor orientation of the ternary complex, or ubiquitinated BTK was not effectively degraded by proteasomes. The detailed mechanism to explain why IRC-1 cannot efficiently degrade BTK requires further investigations. Nonetheless, RC-1, the reversible covalent counterpart of IRC-1, addresses the non-catalytic degradation issue of IRC-1 and brings unexpected intracellular accumulation advantages.

Disrupting the kinase function of BTK using kinase inhibitors is the only currently available therapeutic intervention on this well-validated target. However, it was shown that BTK can enhance antigen receptor-induced calcium influx in a kinase-independent manner [41], while a kinase-inactive BTK mutant can partially rescue B cell development of *BTK* null B cells in mice [42]. Additionally, conditional mouse knockouts of *BTK* after the establishment of B-cell populations have shown that B-cell populations were maintained in conditional knockout mice [43], suggesting that BTK may not be essential for the survival of mature, normal human B-cells. This work supports the hypothesis that BTK degradation will have little effect on normal human B-cells but will result in the

cell death of MCL and CLL cells, which rely on BTK for survival and proliferation. In this work, we developed a small molecule therapeutic agent that can efficiently inhibit and degrade BTK irrespective of *BTK* mutation status to abolish both BTK kinase and non-kinase activities completely**.** It should be noted that although a few BTK degraders have been reported [13, 22, 24, 25, 26], they have low target engagement due to their poor intracellular accumulation (**Figure 4D**). It is usually very difficult for degraders to achieve 100% degradation of the target protein, and the remaining small portion of undegraded BTK can be sufficient to sustain the signaling cascades due to its enzymatic nature. Clinically, it is important for ibrutinib to achieve 100% BTK engagement to completely shut down the BTK downstream signaling. In terms of BTK degradation, RC-1 is more potent than MT-802 at a low concentration (8 nM) and has a comparable potency at a high concentration (200 nM) (**Supplementary Figure 11**). However, our BTK degrader RC-1 is unique compared with other BTK degraders because it not only degrades BTK efficiently but also shows high target engagement to inhibit BTK in case BTK is not completely degraded. This novel dual mechanism of action (MOA) for BTK inhibition and degradation has never been explored in the clinic.

While we are submitting the manuscript, the London group released a ChemRxiv preprint comparing the reversible covalent, irreversible covalent and reversible noncovalent BTK degraders [44]. In their study, the reversible covalent BTK PROTAC was not very potent in protein degradation assays compared with the irreversible covalent and reversible noncovalent counterparts. The main difference between our reversible covalent PROTAC and theirs is the dimethyl group at the γ-position of the cyanoacrylamide group in RC-1, which reduces the reactivity of the Michael acceptor, leading a mM K_d when reacting with small molecule thiols. The cyanoacrylamide in London's reversible covalent PROTACs is too reactive towards small molecule thiols. We speculate that due to the high reactivity of London's reversible covalent PROTACs, they may react with cysteine in the medium even before entering cells, thus reducing the intracellular concentration of the PROTACs. In their final published paper [45], they showed that adding the dimethyl group to their initial reversible covalent BTK PROTAC indeed significantly increased its potency. There are still some discrepancies between their and our studies. Intriguingly, they showed that the irreversible covalent PROTAC can degrade both wild type BTK and the C481S mutant, while the reversible covalent PROTAC can only degrade wild type BTK not the C481S mutant. In our study, we found that RC-1 degrades both wild type BTK and the C481S mutant with similar potency. Additionally, they showed that their reversible covalent and reversible non-covalent PROTACs have similar

cellular concentrations based on a lysate-based LCMS measurement, contrary to our measurements of RC-1 and RNC-1 using the live cell based NanoBRET assay. It should be noted that the PROTAC molecules used in these two studies are not the same, particularly the linker lengths. The linker optimization we performed was focused on reversible covalent PROTACs. It is potentially possible that reversible noncovalent BTK PROTACs may have a different optimal linker length from the reversible covalent counterparts. It would be interesting to compare London's and our BTK PROTACs in the same target engagement and BTK degradation assays before a general conclusion could be drawn whether reversible covalent PROTACs are advantageous than the reversible noncovalent counterparts.

In summary, we have not only developed a unique dual-functional BTK inhibitor and degrader but also provided a general strategy to improve intracellular accumulation of PROTACs and other small molecules with poor cellular permeability. We are the first to apply reversible covalent chemistry to develop PROTACs and serendipitously discovered that the reversible covalent cyano-acrylamide moiety can enhance intracellular accumulation of compounds. Our approach provides a potential solution to address intracellular accumulation issues, a major problem of PROTAC development, and could be generally applied to other small molecule drugs with molecular weight > 500. Unlike other PROTACs with low target occupancy due to poor permeability, RC-1 has high target occupancy and is effective as both an inhibitor and a degrader. This feature is highly important to ensure undegraded BTK protein would still be inhibited by RC-1. Otherwise, the remaining small portion of undegraded BTK can be sufficient to support the signaling cascades due to its catalytic nature. Additionally, molecular dynamics calculations and phase-separation based ternary complex assays also support that RC-1 forms a stable ternary complex with BTK and CRBN. Last but not least, RC-1 compares favorably with other reported BTK degraders in cell viability and target engagement assays and has a reasonable plasma half-life for *in vivo* applications. We hope this work can not only help to develop optimal BTK degraders for clinical applications but also provide a new strategy to improve PROTAC efficacy.

Conflict of Interests

J.W., W.G., X.Q., M.L.W., K.N., and Y.L. are the co-inventors of a patent related to this work. Additionally, J.W. is the co-founder of CoActigon Inc. and Chemical Biology Probes LLC.

Acknowledgment

The research was supported in part by National Institute of Health (R01-GM115622 and R01-CA250503 to J.W.), Baylor College of Medicine (seed funding to J.W.) and Howard Hughes Medical Institute (to M.C.W.). Work at the Center for Theoretical Biological Physics sponsored by the NSF (Grants PHY-1427654 and CHE-1614101) and by the Welch Foundation (Grant C-1792). J.N.O. is a Cancer Prevention and Research Institute of Texas (CPRIT) Scholar in Cancer Research. We also thank Dr. Alex Rosa Campos at the Proteomics Core (supported by NIH P30 CA030199) from Sanford Burnham Prebys for his help with the proteomics experiment, Dr. Matthew Calabrese at Pfizer for sharing the plasmid sequences of truncated CRBN, Dr. Yulin Li at Houston Methodist Research Institute for providing the B cell lymphoma cell line derived from Eu-Myc mice, and Drs. Danette Daniels and Jim Vasta at Promega for their advice on the NanoBRET assays.

Data Availability

Supplementary methods and materials, figures and tables are available. All mass spectrometry raw files been deposited in the MassIVE repository housed at UCSD (https://massive.ucsd.edu/) with the accession number MSV000084902. Direct ftp download is available here ftp://massive.ucsd.edu/MSV000084902/. The source data underlying all supplementary figures and tables are provided as the Source Data file. All other data are available from the corresponding authors on reasonable request.

Author Contributions

W.G, X.Q., and J.W. conceived the idea and design of the study. W.G, X.Q., X.Y., Y.L., C.C, F.B., X.L, D.L, L.W., J.C., and L.H.S. performed the experiments. F.L., M.C.W., X.S., J.N.O., J.A.W., and M.L.W. provided reagents. W.G, X.Q., K.J.N., M.L.W., and J.W. analyzed the data and wrote the manuscript.

Table 1. BTK inhibition, In-Cell Target Engagement and Cell Viability

Compound	K_d (nM) [a]	BTK Inhibition IC_{50} (nM) [b]	Cell Viability IC_{50} (μM) [c]	BTK TE $IC_{50,TE}$ (μM) [d]	$K'_{P,D}$ [e]
RC-1	6.4	1.8	0.31	0.043	1.5×10^{-1}
IRC-1	3.0	0.8	2.7	0.13	2.3×10^{-2}
RNC-1	4.7	21.2	4.1	1.27	3.7×10^{-3}
RC-1-Me		6.8	0.21		
RC-Ctrl	9.1	2.2	0.50	0.054	1.7×10^{-1}
IRC-Ctrl		0.3	0.33		
RNC-Ctrl		13.6	0.42		
RNC-CN-DiMe	29			0.93	3.1×10^{-2}
IRC-DiMe	11			0.38	2.9×10^{-2}

a. The dissociation equilibrium constant K_d was measured using the full-length BTK protein by Eurofins DiscoverX. The reported K_d values for RC-1, IRC-1 and RC-Ctrl were measured in the absence of DTT in the buffer. DTT (6 mM) used in the standard assay condition increases the K_d values of RC-1 and RC-ctrl by 2-3 folds, while it does not affect the measurement for IRC-1. The reported K_d value for RNC-1 was measured in the standard assay buffer with the presence of DTT. Duplicates were performed. The assay procedure is provided in a Source Data file.

b. The biochemical BTK inhibition (BTK Inhibition IC_{50}) was measured using the BTK assay kit from AssayQuant Technologies Inc. Duplicates were performed.

c. Cell viability IC_{50} was performed by treating MOLM-14 cells with compounds for 72 h, followed by Alamar Blue assays.

d. BTK Target Engagement IC_{50} is the concentration of an unlabeled compound that results in a half-maximal inhibition binding of the BTK tracer. The target engagement of compounds was assessed following Promega's assay protocol. Triplicates were performed.

e. $K'_{P,D}$ is a relative intracellular accumulation coefficient for drug D and calculated as $K_d/IC_{50,TE}$. $K'_{P,D}$ is an assay-dependent parameter to quantify the tendency of intracellular accumulation of a drug. Under the same assay conditions, a greater $K'_{P,D}$ value for a drug reflects its higher tendency to accumulate inside cells. Please refer to the supporting information for detailed explanation.

Table 2. CRBN Binding and In-Cell Target Engagement

Compound	K_d (μM) [a]	$IC_{50,TE}$ (μM) [b]	$K'_{P,D}$ [c]
RC-1	4.2	0.25	16.8
IRC-1	1.5	0.86	1.7
RNC-1	1.8	1.69	1.1
Pomalidomide	1.4	0.30	4.7

a. The dissociation equilibrium constant K_d was measured using a truncated Cereblon protein. Triplicates were performed. The assay procedure is provided in the Source Data files.

b. CRBN Target Engagement IC_{50} is the concentration of an unlabled compound that results in a half-maximal inhibition binding of the CRBN tracer. The target engagement of compounds was assessed following Promega's assay protocol. Triplicates were performed.

c. $K'_{P,D}$ is a relative intracellular accumulation coefficient for drug D and calculated as $K_d/IC_{50,TE}$. $K'_{P,D}$ is an assay-dependent parameter to quantify the tendency of intracellular accumulation of a drug. Under the same assay conditions, a greater $K'_{P,D}$ value for a drug reflects its higher tendency to accumulate inside cells. Please refer to the supporting information for detailed explanation.

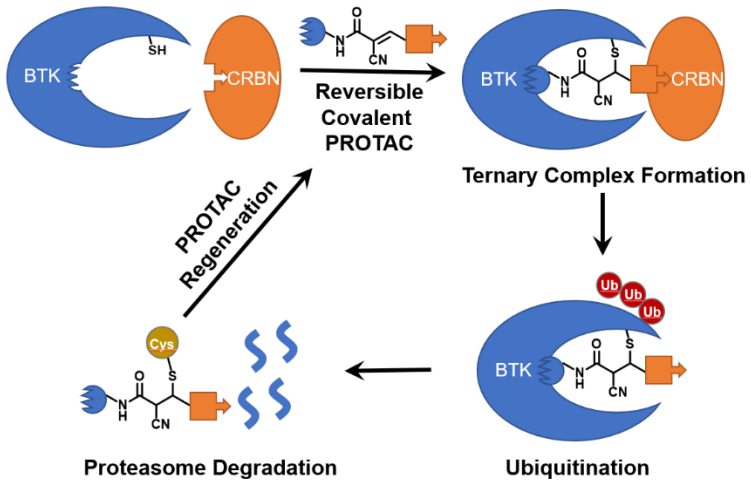

Figure 1. Demonstration of catalytic degradation of targeted proteins by reversible covalent PROTACs. The premise of this reversible covalent PROTAC design is the weak reactivity (mM K_d) between α-cyano-acrylamide group (the chemical structure shown above) and free thiols. Only when the PROTAC molecule binds to the active site of the targeted protein, the nearby cysteine side chain can react with the α-cyano-acrylamide group to form a stable covalent bond. Once the targeted protein is degraded, the reversible covalent PROTAC can be regenerated.

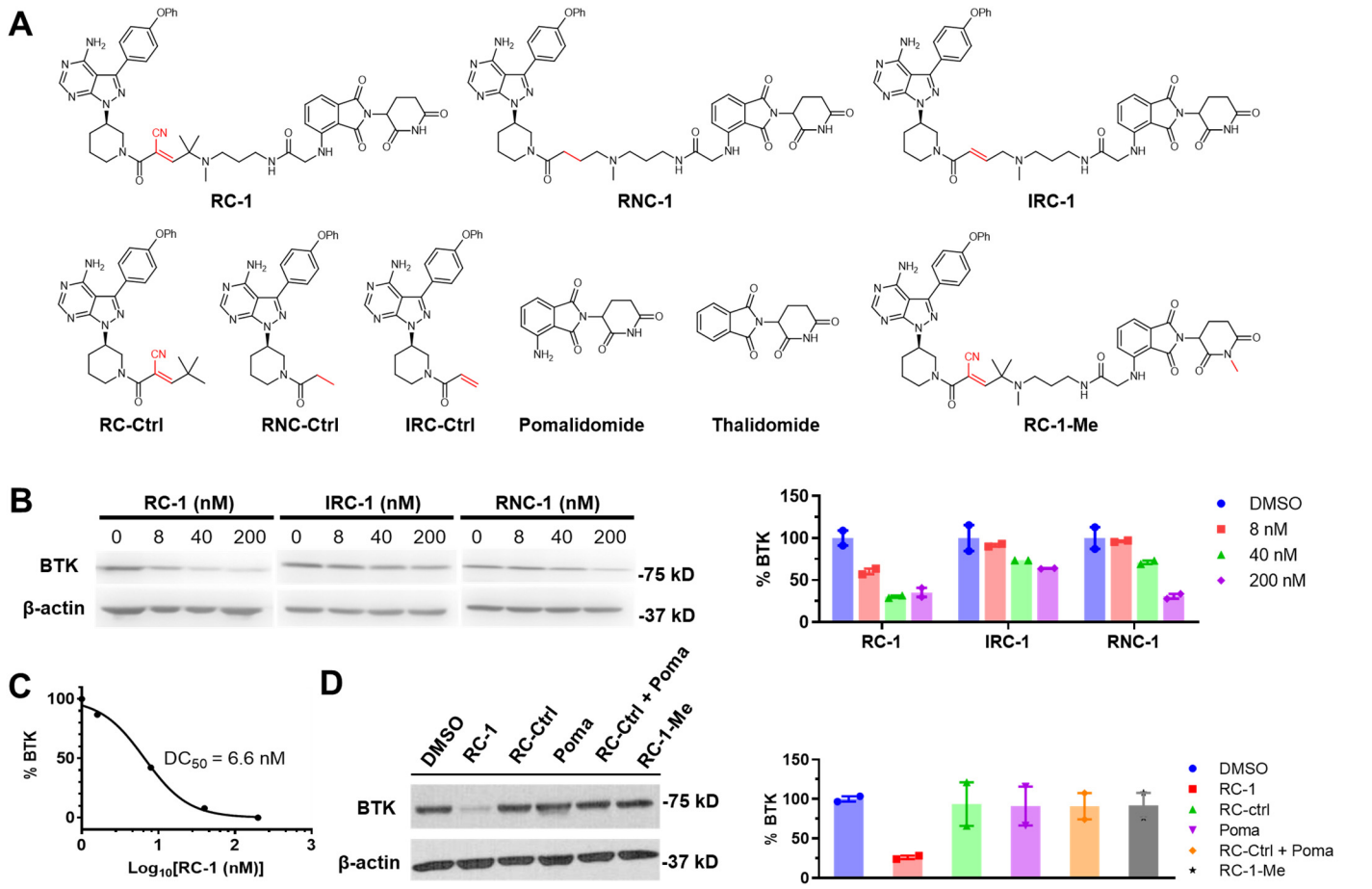

Figure 2. BTK degradation induced by PROTACs. (A) Chemical structures of BTK degraders and their controls. RC-1, RNC-1 and IRC-1 are BTK degraders with reversible covalent, reversible non-covalent, and irreversible covalent warheads, respectively. RC-Ctrl, RNC-Ctrl, and IRC-Ctrl (i.e., ibrutinib) are the corresponding warhead controls for RC-1, RNC-1 and IRC-1, respectively. (B) MOLM-14 cells were incubated with RC-1, RNC-1 and IRC-1 for 24 h. The BTK levels were quantified by Western blotting. Duplicates were performed with SEM as the error bars. (C) RC-1 dose-dependent BTK degradation in MOLM-14 cells. DC_{50}: compound concentration inducing 50% of protein degradation. (D) MOLM-14 cells were treated with DMSO, RC-1, RC-Ctrl, Pomalidomide, RC-Ctrl + Pomalidomide, and RC-1-Me for 24 h. All the compound concentrations are 200 nM. Neither RC-Ctrl, nor pomalidomide, nor a combination of both caused BTK degradation, indicating that the bifunctional PROTAC molecule is essential to facilitate the formation of a ternary complex of {BTK-PROTAC-CRBN} in order to induce BTK degradation. Duplicates were performed with SEM as the error bars. The raw data are provided as a Source Data file.

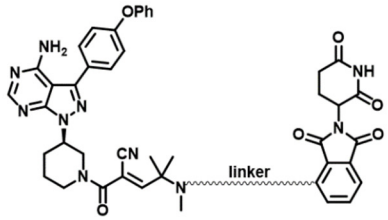

Compound	Linker	Degradation at 200 nM
RC-1	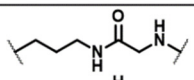	81%
RC-2	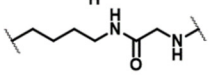	49%
RC-3	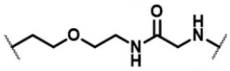	39%
RC-4	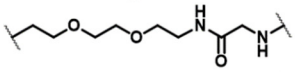	43%
RC-5	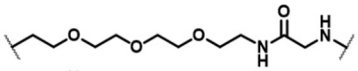	56%
RC-6	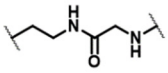	--
RC-7	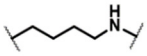	6%
RC-8	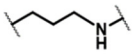	15%
RC-9	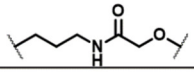	30%

Figure 3. Linker optimization for reversible covalent BTK degraders. Optimization of the linkers of the RC series of BTK degraders and their corresponding % of BTK degradation in MOLM-14 cells (200 nM, 24 h incubation). Note: RC-6 was unstable due to intramolecular cyclization with the Michael acceptor.

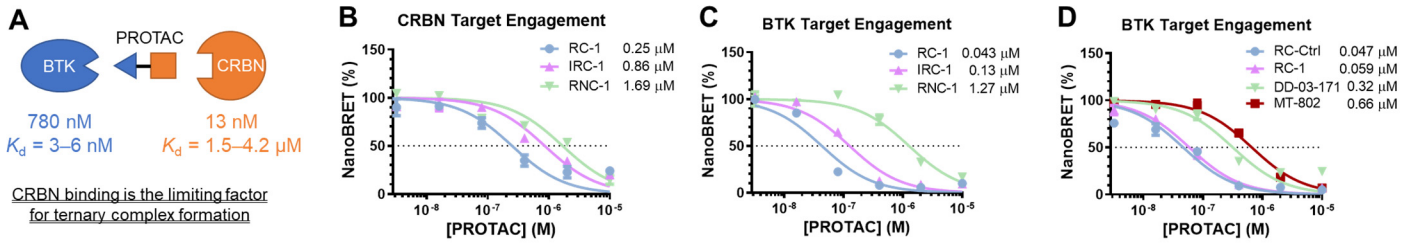

Figure 4. Target engagement for BTK degraders. (A) Quantitative Western blot was performed on lysate of 1×10^6 MOLM-14 cells using BTK and CRBN recombinant proteins as the standard. Assuming the MOLM-14 volume is 1000 μM^3, we can calculate the BTK and CRBN concentrations are 780 and 13 nM, respectively. Considering the weak binding between pomalidomide and CRBN, we can conclude that CRBN binding is the limiting factor for ternary complex formation. (B) CRBN in-cell target engagement assay. HEK-293 cells were transiently transfected with plasmids expressing a fusion protein of CRBN and nano-luciferase (nLuc) for 24 h and then the cells were treated with a CRBN tracer (0.5 μM), which binds to CRBN to induce bioluminescence resonance energy transfer (BRET). Adding PROTACs to cells would compete the CRBN tracer binding to CRBN, thus reducing the NanoBRET signals. It should be noted that the NanoBRET assay is ratiometric and independent of the expression level of the nLuc fusion protein. The target engagement IC_{50} values for RC-1, IRC-1, and RNC-1 are 0.25, 0.86. and 1.69 μM, respectively. (C) BTK in-cell target engagement assay. This assay is the same as the CRBN in-cell target engagement assay, except BTK-nLuc fusion plasmid and BTK tracer (1.0 μM) were used. The target engagement IC_{50} values for RC-1, IRC-1, and RNC-1 are 0.043, 0.13 and 1.27 μM, respectively. (D) The same BTK in-cell target engagement assay as in (C) was applied to RC-1, RC-Ctrl, DD-03-171 and MT-802. The target engagement IC_{50} values for RC-1 and RC-Ctrl are the same within experimental errors, demonstrating that the intracellular accumulation of RC-1 is similar to its parent warhead molecule. In contrast, the target engagement IC_{50} values for DD-03-171 and MT-802 are 5 and 11 folds of that of RC-1, respectively. Triplicates were performed with SEM as the error bars. The raw data are provided as a Source Data file.

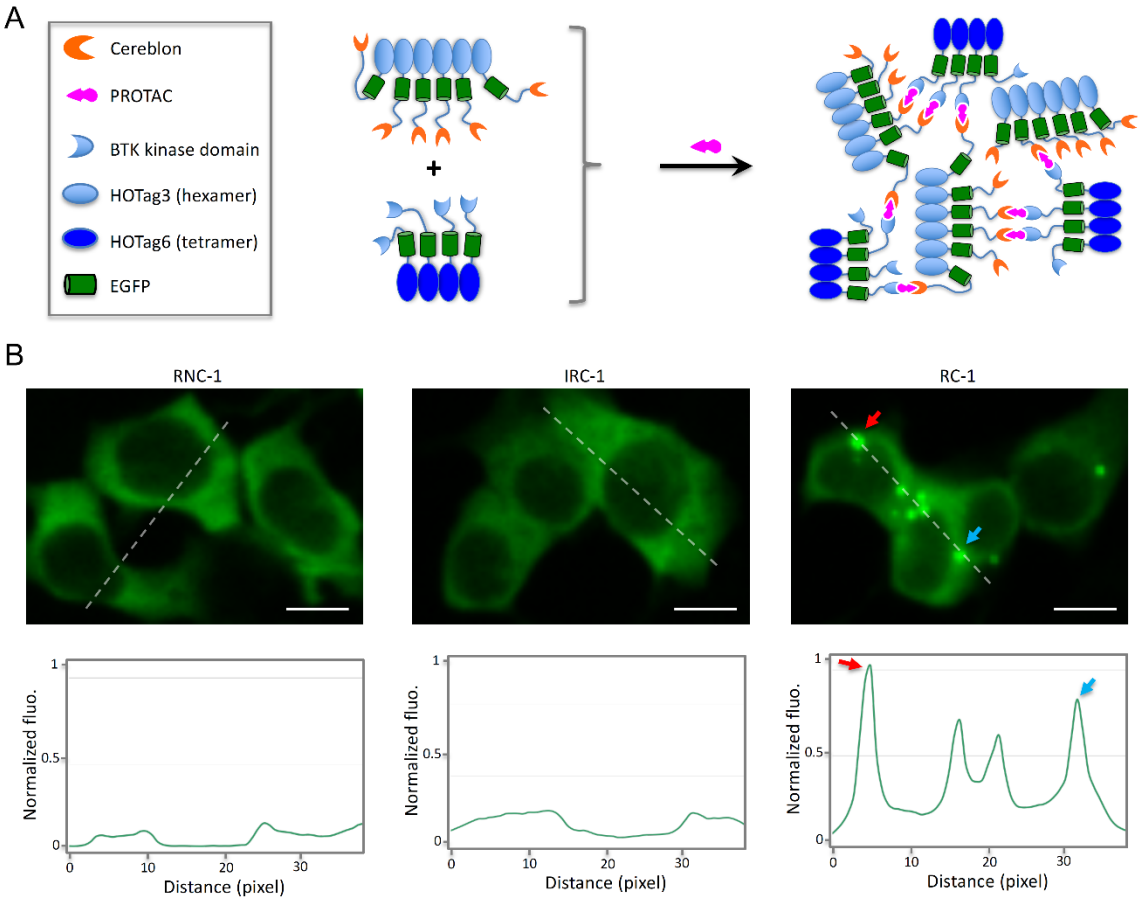

Figure 5. Fluorophore phase separation-based assay for imaging ternary complex formation in living cells. (A) Schematic diagram showing the design of the cellular assay. To detect PROTAC-induced PPI between BTK and CRBN, we engineered the kinase domain of BTK (amino acid residues 382 – 659, referred to as BTK^{KD}) into SPPIER to produce a BTK^{KD}-EGFP-HOTag6 construct, which forms tetramers when expressing in cells. The previously reported CRBN-EGFP-HOTag3 fusion construct, which forms hexamers in cells, was used as the E3 ligase SPPIER. If PROTACs can induce {BTK-PROTAC-CRBN} ternary complex formation in cells, they will crosslink the BTK^{KD}-EGFP-HOTag6 tetramers and the CRBN-EGFP-HOTag3 hexamers to produce EGFP phase separation, which can be conveniently visualized with a fluorescence microscope. (B) Fluorescence images showing detection of BTK PROTACs-induced interaction between the E3 ligase cereblon and the target protein BTK. A fluorescence histogram of the line across the cells is shown below. HEK293 cells transiently expressed BTK^{KD}-EGFP-HOTag6 and CRBN-EGFP-HOTag3. RC-1, IRC-1 and RNC-1 (10 μM) were added to the cells. Scale bar: 10 μm. Please contact Dr. Xiaokun Shu (xiaokun.shu@ucsf.edu) for assay details.

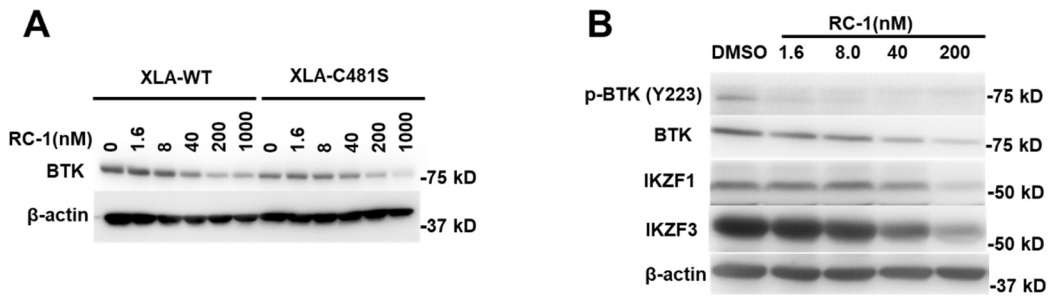

Figure 6. RC-1 overcomes drug resistance. (A) XLA cells overexpressing wild type or C481S mutant BTK were treated with RC-1 for 24 h. Then Western blotting was performed to evaluate the degradation of BTK. Duplicates were performed. (C) RC-1 induced degradation of BTK, pBTK, IKZF1 and IKZF3 in Mino cells. Duplicates were performed. The raw data are provided as a Source Data file.

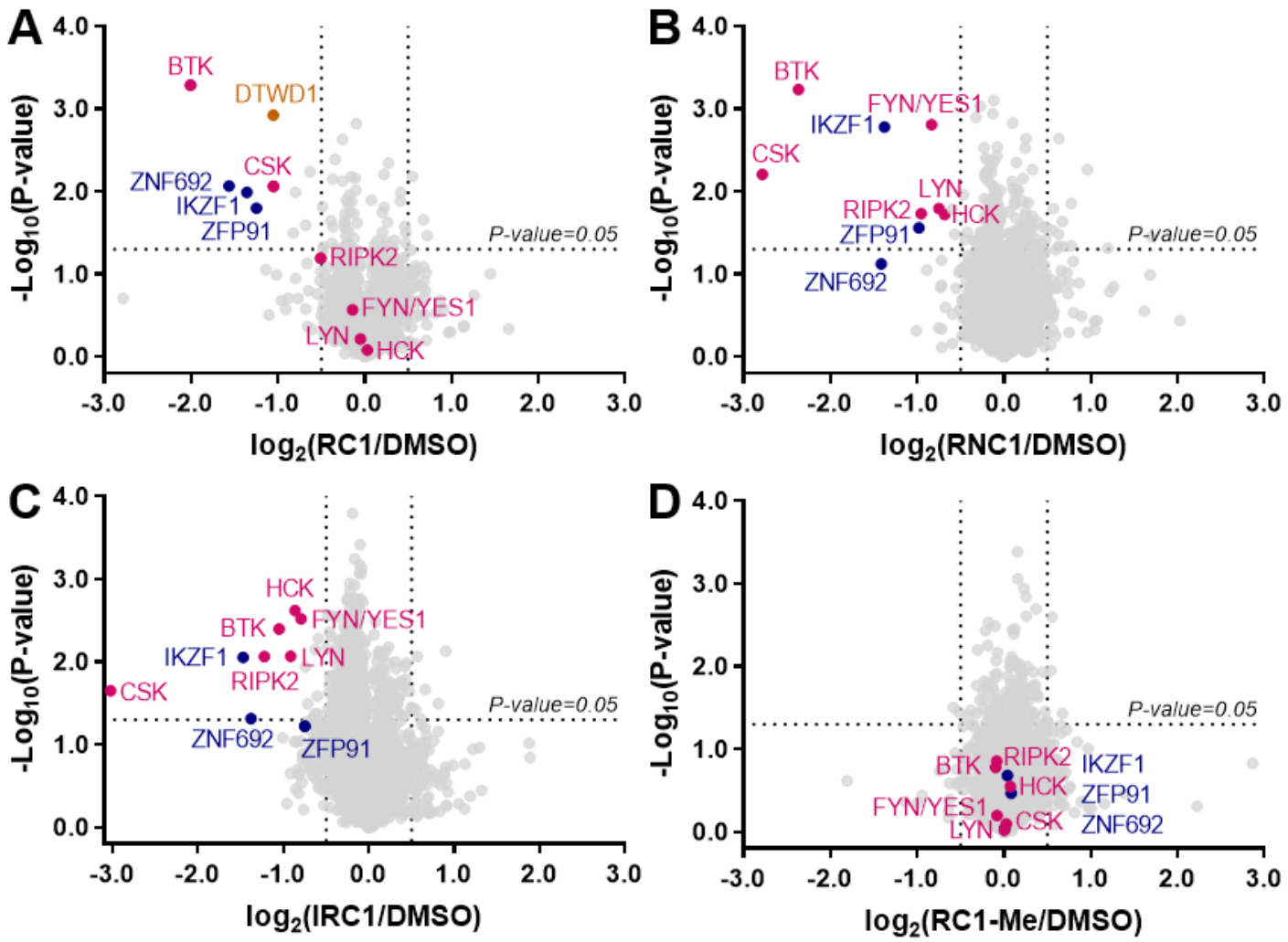

Figure 7. Proteomic analysis showing RC-1 selectively degrades BTK. MOLM-14 cells were treated with either compounds [200 nM (A) RC-1, (B) RNC-1, (C) IRC-1, or (D) RC-1-Me (RC-1 non-degrader control)] or DMSO for 24 h. Lysates were treated with a TMT-10plex kit and subjected to mass spec-based proteomics analysis. Datasets represent an average of duplicates. Volcano plot shows protein abundance (log2) as a function of significance level (log10). Nonaxial vertical lines denote abundance changes from 0.7 to 1.4 (i.e. $2^{\pm 0.5}$), whereas nonaxial horizontal line marks P = 0.05 significance threshold. Downregulated proteins of significance are found in the upper left quadrant of the plots. Violet red dots represent kinases. Dark blue dots represent zinc finger proteins. Both RNC-1 and IRC-1 showed significant degradation of 7 kinases, while RC-1 only degrades BTK and CSK. A total of 7,280 proteins were identified, and only the ones with at least one uniquely identified peptide are displayed. The raw data are provided as a Source Data file.

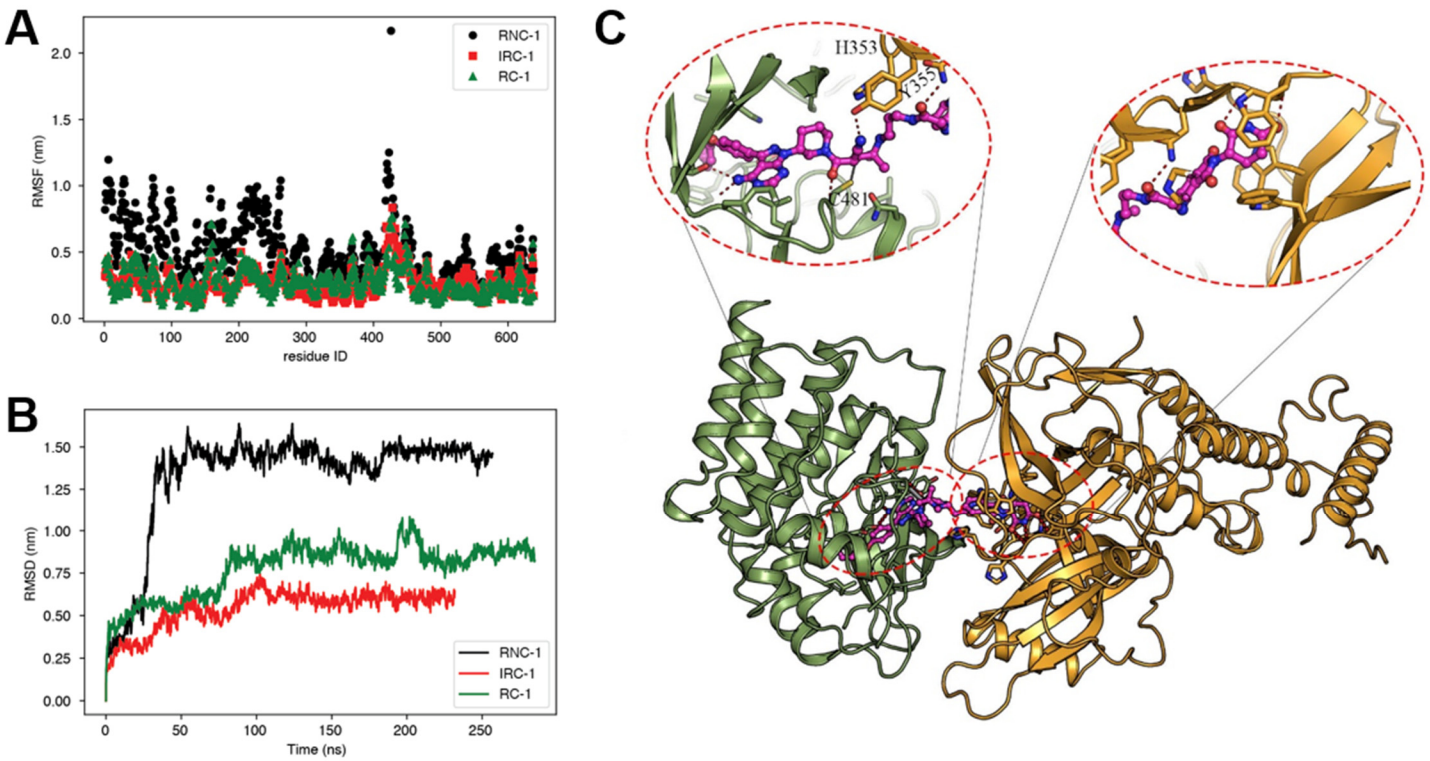

Figure 8. Molecular dynamics simulations for ternary complexes of BTK-PROTAC-CRBN. (A) RNC-1 mediated complex shows a larger structural fluctuation compared with the other two ligands, reflected by (A) Root Mean Square Fluctuation (RMSF) per residue and (B) Root Mean Square Deviation (RMSD) calculated from the simulations of the {BTK-PROTAC-CRBN} ternary complexes. (C) Predicted most stable conformation of {BTK-RC-1-CRBN} ternary complex. Red dashes indicate the hydrogen bonds formed among the ligand, proteins, or waters. Light green cartoons are BTK and cyan cartoons are E3 ligase. Magenta stick ball models represent RC-1.

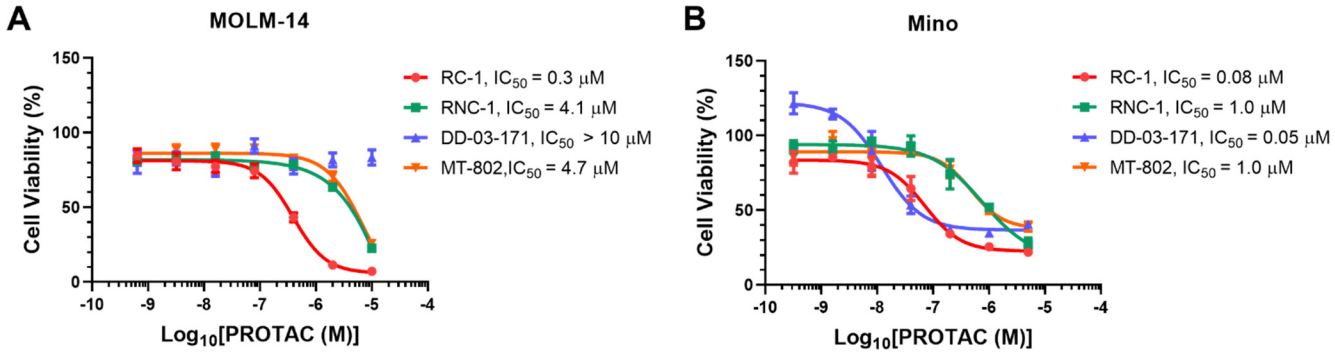

Figure 9. Comparison of RC-1 with other reported BTK degraders. Two previously reported BTK degraders DD-03-171 and MT-802 were synthesized in house. The cells were treated with compounds for 72 h. Then Alarma blue assays were performed to quantify the cellular viabilities. Data are presented as means ± SEM of 5 replicates. The raw data are provided as a Source Data file.

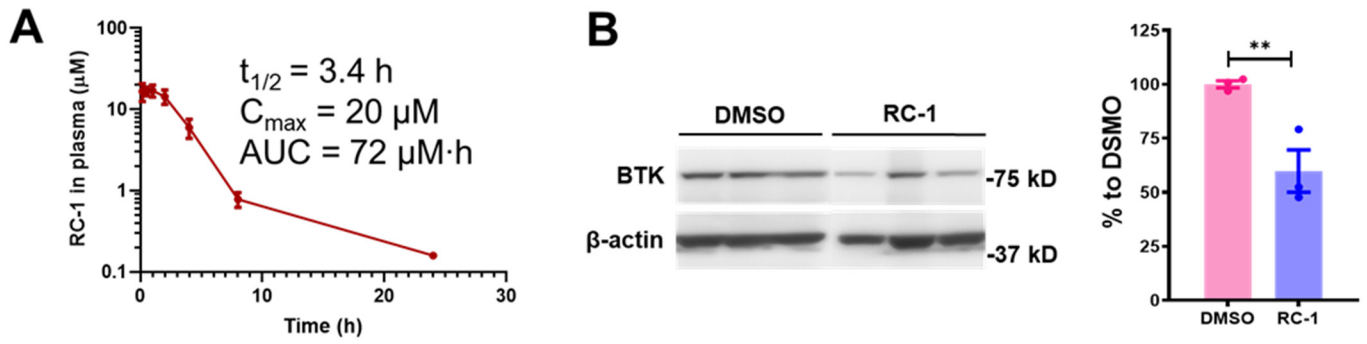

Figure 10. PK/PD of RC-1. (A) RC-1 (20 mg/kg, single i.p. injection) in ICR mice plasma (n=3). (B) Representative western blot (left) and quantification (right) of splenic BTK level in mice (n=3) treated with 7 once daily i.p. injection of 20 mg/kg RC-1 (spleens were harvested 24 h after the 7th injection). The raw data are provided as a Source Data file.

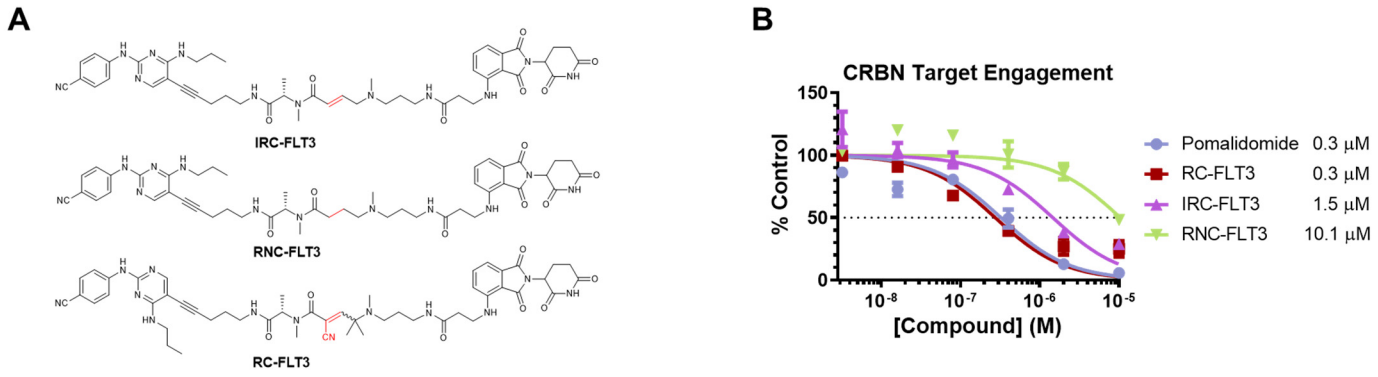

Figure 11. Target engagement for FLT3 degraders. (A) Chemical structures of FLT3 degraders. (B) CRBN in-cell target engagement assay. HEK-293 cells were transiently transfected with plasmids expressing a fusion protein of CRBN and nano-luciferase (nLuc) for 24 h and then the cells were treated with a CRBN tracer (0.5 μM), which binds to CRBN to induce energy transfer signals. Adding drugs to cells would compete the CRBN tracer binding to CRBN, thus reducing the NanoBRET signals. The target engagement IC_{50} values for pomalidomide, RC-FLT3, IRC-FLT3 and RNC-FLT3 are 0.3, 0.3, 1.5 and 10.1 μM, respectively. Triplicates were performed with SEM as the error bars. The raw data are provided as a Source Data file.

References

1. Burslem GM, Crews CM. Small-Molecule Modulation of Protein Homeostasis. *Chemical reviews* **117**, 11269-11301 (2017).

2. Sakamoto KM, Kim KB, Kumagai A, Mercurio F, Crews CM, Deshaies RJ. Protacs: chimeric molecules that target proteins to the Skp1-Cullin-F box complex for ubiquitination and degradation. *Proceedings of the National Academy of Sciences of the United States of America* **98**, 8554-8559 (2001).

3. Scudellari M. Protein-slaying drugs could be the next blockbuster therapies. *Nature* **567**, 298-300 (2019).

4. Bondeson DP*, et al.* Catalytic in vivo protein knockdown by small-molecule PROTACs. *Nature chemical biology* **11**, 611-617 (2015).

5. Burslem GM*, et al.* The Advantages of Targeted Protein Degradation Over Inhibition: An RTK Case Study. *Cell chemical biology* **25**, 67-77 e63 (2018).

6. Graves LM, Duncan JS, Whittle MC, Johnson GL. The dynamic nature of the kinome. *Biochem J* **450**, 1-8 (2013).

7. Leiser D*, et al.* Targeting of the MET receptor tyrosine kinase by small molecule inhibitors leads to MET accumulation by impairing the receptor downregulation. *FEBS Lett* **588**, 653-658 (2014).

8. Gadd MS*, et al.* Structural basis of PROTAC cooperative recognition for selective protein degradation. *Nature chemical biology* **13**, 514-521 (2017).

9. Smith BE*, et al.* Differential PROTAC substrate specificity dictated by orientation of recruited E3 ligase. *Nature communications* **10**, 131 (2019).

10. Jiang B*, et al.* Development of Dual and Selective Degraders of Cyclin-Dependent Kinases 4 and 6. *Angewandte Chemie* **58**, 6321-6326 (2019).

11. Brand M*, et al.* Homolog-Selective Degradation as a Strategy to Probe the Function of CDK6 in AML. *Cell chemical biology* **26**, 300-306 e309 (2019).

12. Bai L*, et al.* A Potent and Selective Small-Molecule Degrader of STAT3 Achieves Complete Tumor Regression In Vivo. *Cancer cell* **36**, 498-511 e417 (2019).

13. Tinworth CP*, et al.* PROTAC-Mediated Degradation of Bruton's Tyrosine Kinase Is Inhibited by Covalent Binding. *ACS chemical biology* **14**, 342-347 (2019).

14. Buckley DL*, et al.* HaloPROTACS: Use of Small Molecule PROTACs to Induce Degradation of HaloTag Fusion Proteins. *ACS chemical biology* **10**, 1831-1837 (2015).

15. Jiang X*, et al.* Quantitative Real-Time Imaging of Glutathione with Subcellular Resolution. *Antioxidants & redox signaling* **30**, 1900-1910 (2019).

16. Jiang X*, et al.* Quantitative real-time imaging of glutathione. *Nature communications* **8**, 16087 (2017).

17. Jiang X*, et al.* Quantitative imaging of glutathione in live cells using a reversible reaction-based ratiometric fluorescent probe. *ACS chemical biology* **10**, 864-874 (2015).

18. Chen J*, et al.* Reversible Reaction-Based Fluorescent Probe for Real-Time Imaging of Glutathione Dynamics in Mitochondria. *ACS Sens* **2**, 1257-1261 (2017).

19. Bradshaw JM*, et al.* Prolonged and tunable residence time using reversible covalent kinase inhibitors. *Nature chemical biology* **11**, 525-531 (2015).

20. Woyach JA*, et al.* Resistance mechanisms for the Bruton's tyrosine kinase inhibitor ibrutinib. *The New England journal of medicine* **370**, 2286-2294 (2014).

21. Johnson AR*, et al.* Battling Btk Mutants With Noncovalent Inhibitors That Overcome Cys481 and Thr474 Mutations. *ACS chemical biology* **11**, 2897-2907 (2016).

22. Sun Y*, et al.* PROTAC-induced BTK degradation as a novel therapy for mutated BTK C481S induced ibrutinib-resistant B-cell malignancies. *Cell Res* **28**, 779-781 (2018).

23. Huang HT*, et al.* A Chemoproteomic Approach to Query the Degradable Kinome Using a Multi-kinase Degrader. *Cell chemical biology* **25**, 88-99 e86 (2018).

24. Zorba A*, et al.* Delineating the role of cooperativity in the design of potent PROTACs for BTK. *Proceedings of the National Academy of Sciences of the United States of America* **115**, E7285-E7292 (2018).

25. Buhimschi AD*, et al.* Targeting the C481S Ibrutinib-Resistance Mutation in Bruton's Tyrosine Kinase Using PROTAC-Mediated Degradation. *Biochemistry* **57**, 3564-3575 (2018).

26. Dobrovolsky D*, et al.* Bruton tyrosine kinase degradation as a therapeutic strategy for cancer. *Blood* **133**, 952-961 (2019).

27. Crew AP*, et al.* Identification and Characterization of Von Hippel-Lindau-Recruiting Proteolysis Targeting Chimeras (PROTACs) of TANK-Binding Kinase 1. *Journal of medicinal chemistry* **61**, 583-598 (2018).

28. Brown GC. Total cell protein concentration as an evolutionary constraint on the metabolic control distribution in cells. *Journal of theoretical biology* **153**, 195-203 (1991).

29. Douglass EF, Jr., Miller CJ, Sparer G, Shapiro H, Spiegel DA. A comprehensive mathematical model for three-body binding equilibria. *Journal of the American Chemical Society* **135**, 6092-6099 (2013).

30. Chung CI, Zhang Q, Shu X. Dynamic Imaging of Small Molecule Induced Protein-Protein Interactions in Living Cells with a Fluorophore Phase Transition Based Approach. *Anal Chem* **90**, 14287-14293 (2018).

31. Riching KM*, et al.* Quantitative Live-Cell Kinetic Degradation and Mechanistic Profiling of PROTAC Mode of Action. *ACS chemical biology* **13**, 2758-2770 (2018).

32. Robers MB*, et al.* Target engagement and drug residence time can be observed in living cells with BRET. *Nature communications* **6**, 10091 (2015).

33. Mateus A, Treyer A, Wegler C, Karlgren M, Matsson P, Artursson P. Intracellular drug bioavailability: a new predictor of system dependent drug disposition. *Scientific reports* **7**, 43047 (2017).

34. Zhang Y, Huo M, Zhou J, Xie S. PKSolver: An add-in program for pharmacokinetic and pharmacodynamic data analysis in Microsoft Excel. *Comput Methods Programs Biomed* **99**, 306-314 (2010).

35. Yamaura T*, et al.* A novel irreversible FLT3 inhibitor, FF-10101, shows excellent efficacy against AML cells with FLT3 mutations. *Blood* **131**, 426-438 (2018).

36. Krishnan S, Miller RM, Tian B, Mullins RD, Jacobson MP, Taunton J. Design of reversible, cysteine-targeted Michael acceptors guided by kinetic and computational analysis. *Journal of the American Chemical Society* **136**, 12624-12630 (2014).

37. Gasparini G, Sargsyan G, Bang EK, Sakai N, Matile S. Ring Tension Applied to Thiol-Mediated Cellular Uptake. *Angewandte Chemie* **54**, 7328-7331 (2015).

38. Abegg D*, et al.* Strained Cyclic Disulfides Enable Cellular Uptake by Reacting with the Transferrin Receptor. *Journal of the American Chemical Society* **139**, 231-238 (2017).

39. Gemechu Y*, et al.* Humanized cereblon mice revealed two distinct therapeutic pathways of immunomodulatory drugs. *Proceedings of the National Academy of Sciences of the United States of America* **115**, 11802-11807 (2018).

40. Fink EC*, et al.* Crbn (I391V) is sufficient to confer in vivo sensitivity to thalidomide and its derivatives in mice. *Blood* **132**, 1535-1544 (2018).

41. Saito K*, et al.* BTK regulates PtdIns-4,5-P2 synthesis: importance for calcium signaling and PI3K activity. *Immunity* **19**, 669-678 (2003).

42. Middendorp S, Dingjan GM, Maas A, Dahlenborg K, Hendriks RW. Function of Bruton's tyrosine kinase during B cell development is partially independent of its catalytic activity. *J Immunol* **171**, 5988-5996 (2003).

43. Nyhoff LE, Clark ES, Barron BL, Bonami RH, Khan WN, Kendall PL. Bruton's Tyrosine Kinase Is Not Essential for B Cell Survival beyond Early Developmental Stages. *J Immunol* **200**, 2352-2361 (2018).

44. Ronen G*, et al.* Efficient targeted degradation via reversible and irreversible covalent PROTACs. *ChemRxiv11494398v1*, (2020).

45. Gabizon R*, et al.* Efficient Targeted Degradation via Reversible and Irreversible Covalent PROTACs. *Journal of the American Chemical Society*, (2020).